THE JOURNAL OF BIOLOGICAL CHEMISTRY VOL. 281, NO. 52, pp. 40224–40235, December 29, 2006

Kinetic Analysis of Interaction of Eukaryotic Release Factor 3 with Guanine Nucleotides*

Received for publication, August 4, 2006, and in revised form, October 23, 2006 Published, JBC Papers in Press, October 24, 2006, DOI 10.1074/jbc.M607461200

Vera P. Pisareva[‡], Andrey V. Pisarev[‡], Christopher U. T. Hellen[‡], Marina V. Rodnina[§1], and Tatyana V. Pestova[‡¶2]

From the [‡]Department of Microbiology and Immunology, State University of New York Downstate Medical Center, Brooklyn, New York 11203, the [§]Institute of Physical Biochemistry, University of Witten/Herdecke, 58448 Witten, Germany, and the [¶]A. N. Belozersky Institute of Physico-Chemical Biology, Moscow State University, 119899 Moscow, Russia

Eukaryotic translation termination is mediated by two release factors: eRF1 recognizes stop codons and triggers peptidyl-tRNA hydrolysis, whereas eRF3 accelerates this process in a GTP-dependent manner. Here we report kinetic analysis of guanine nucleotide binding to eRF3 performed by fluorescence stopped-flow technique using GTP/GDP derivatives carrying the fluorescent methylanthraniloyl (mant-) group, as well as thermodynamic analysis of eRF3 binding to unlabeled guanine nucleotides. Whereas the kinetics of eRF3 binding to mant-GDP is consistent with a one-step binding model, the double-exponential transients of eRF3 binding to mant-GTP indicate a two-step binding mechanism, in which the initial eRF3·mant-GTP complex undergoes subsequent conformational change. The affinity of eRF3 for GTP (K_d, ~70 μM) is about 70-fold lower than for GDP (K_d, ~ 1 μM) and both nucleotides dissociate rapidly from eRF3 ($k_{-1}^{\text{mant-GDP}} \sim 2.4\ s^{-1}$; $k_{-2}^{\text{mant-GTP}} \sim 3.3\ s^{-1}$). Whereas not influencing eRF3 binding to GDP, association of eRF3 with eRF1 at physiological Mg^{2+} concentrations specifically changes the kinetics of eRF3/mant-GTP interaction and stabilizes eRF3·GTP binding by two orders of magnitude ($K_d \sim 0.7\ \mu$M) due to lowering of the dissociation rate constant ~24-fold ($k_{-1}^{\text{mant-GTP}} \sim 0.14\ s^{-1}$). Thus, eRF1 acts as a GTP dissociation inhibitor (TDI) for eRF3, promoting efficient ribosomal recruitment of its GTP-bound form. 80 S ribosomes did not influence guanine nucleotide binding/exchange on the eRF1·eRF3 complex. Guanine nucleotide binding and exchange on eRF3, which therefore depends on stimulation by eRF1, is entirely different from that on prokaryotic RF3 and unusual among GTPases.

Termination of protein synthesis occurs when a ribosome reaches the end of the coding region of an mRNA and a stop codon enters the decoding site. Termination is mediated by two classes of release factor (RF)[3] (1). Class I release factors, RF1/RF2 in bacteria and eRF1 in eukaryotes, bind to the A site, recognize the stop codon, and promote hydrolysis of the P-site peptidyl-tRNA, thereby releasing the polypeptide. Class I release factors contain a universally conserved GGQ sequence located in a loop that enters the peptidyl transferase center (2–4) and is required to trigger peptidyl-tRNA hydrolysis (5, 6). Class II release factors, RF3 in bacteria and eRF3 in eukaryotes, are GTPases (7, 8) whose sequence homology is limited to their GTP binding domains (9). In contrast to prokaryotic RF3, activation of eRF3 GTPase activity strictly requires both the 80 S ribosome and eRF1 (10, 11). A distinguishing feature of eukaryotic RFs is that eRF1 and eRF3 form a stable complex through interaction of their C-terminal domains (12, 13), and this physical interaction is required for stimulation of eRF3 GTPase activity by eRF1 on the ribosome (10).

Prokaryotic RF3 mediates recycling of RF1/RF2 from post-termination complexes (6, 14, 15). According to the current model of termination in prokaryotes, RF1 and RF2 bind to pre-termination complexes that contain peptidyl-tRNA in the P site and a stop codon in the A site, and stimulate hydrolysis of peptidyl-tRNA (15). The affinity of RF3 to GDP is three orders of magnitude higher than to GTP (15), and hence the majority of RF3 is expected to be in the GDP-bound form in which it initially binds to termination complexes. After hydrolysis of peptidyl-tRNA, GDP dissociates from RF3, which then rapidly binds GTP. Formation of a high affinity complex between the ribosome and RF3·GTP induces dissociation of RF1/RF2. Finally, RF3-bound GTP is hydrolyzed, and the low affinity RF3·GDP complex dissociates from the ribosome. This model implies that ribosomal post-termination complexes containing RF1 or RF2 act as a guanine nucleotide exchange factor (GEF) for RF3 (15).

It was proposed that eRF3 might play a role similar to that of RF3 by promoting recycling of eRF1 (15). However, recent data suggest that GTP hydrolysis by eRF3 instead couples stop codon recognition and peptidyl-tRNA hydrolysis mediated by eRF1 (16, 17). eRF3 strongly enhances peptide release by eRF1 in the presence of GTP, but not GDP, and abrogates peptide

* This work was supported by National Institutes of Health Grant R01 GM63940 (to T. V. P.). The costs of publication of this article were defrayed in part by the payment of page charges. This article must therefore be hereby marked "*advertisement*" in accordance with 18 U.S.C. Section 1734 solely to indicate this fact.

[1] Supported by the Deutsche Forschungsgemeinschaft, the Alfried Krupp von Bohlen und Halbach-Stiftung, and the Fonds der Chemischen Industrie. To whom correspondence may be addressed: Inst. of Physical Biochemistry, University of Witten/Herdecke, Stockumer Str. 10, 58448 Witten, Germany. Tel.: 49-2302-926205; Fax: 49-2302-926117; E-mail: rodnina@uni-wh.de.

[2] To whom correspondence may be addressed: Dept. of Microbiology & Immunology, SUNY Downstate Medical Center, 450 Clarkson Ave., Box 44, Brooklyn, NY 11203. Tel.: 718-221-6121; Fax: 718-270-2656; E-mail: tatyana.pestova@downstate.edu.

[3] The abbreviations used are: RF, release factor; GEF, guanine nucleotide exchange factor; GDI, GDP-dissociation inhibitor; mant-GDP, 2′/3′-*O*-(*N*-methyl-anthraniloyl)-guanosine-5′-diphosphate; mant-GTP, 2′/3′-*O*-(*N*-methyl-anthraniloyl)-guanosine-5′-triphosphate; FPLC, fast protein liquid chromatography; NTA, nitrilotriacetic acid; FRET, fluorescence resonance energy transfer; GTPγS, guanosine 5′-3-*O*-(thio)triphosphate.

release in the presence of the non-hydrolyzable GTP analog GDPNP even when eRF1 is in large excess, *i.e.* recycling of eRF1 is not required (17). Thus, whereas RF3 increases the rate of RF1/RF2 release from the ribosome, eRF3 seems to ensure rapid and efficient hydrolysis of peptidyl-tRNA by eRF1. Apparently, binding of eRF1, eRF3, and GTP to pretermination ribosomes leads to a complex that is not active in peptide release, and further rearrangement, induced by GTP hydrolysis, is required for proper positioning of the GGQ loop of eRF1 in the peptidyl transferase center (17). Thus, an apparently important difference between prokaryotic and eukaryotic termination mechanisms is that in prokaryotes peptide release precedes and is required for GTP hydrolysis by RF3, whereas in eukaryotes GTP hydrolysis by eRF3 is necessary for the hydrolysis of peptidyl-tRNA and peptide release. The difference in the roles of eukaryotic eRF3 and prokaryotic RF3 in termination suggests that their affinities to GTP and GDP and their mechanisms of GDP/GTP exchange may also differ.

Although the thermodynamics of eRF3 interaction with guanine nucleotides was studied previously using isothermal titration calorimetry (18) and more recently, while this article was being reviewed, by non-equilibrium filter binding technique (19), the kinetics of interaction of eRF3 with guanine nucleotides remained uninvestigated. Here we report a kinetic study of the interaction of guanine nucleotides with eRF3 alone and with the eRF3·eRF1 complex in the absence and in the presence of 80 S ribosomes. Guanine nucleotide binding and dissociation were studied by stopped flow and equilibrium fluorescence titration techniques using unlabeled GTP/GDP and their derivatives carrying the fluorescent methylanthraniloyl (mant-) group. Our studies revealed that mutual interdependence of eRF1 and eRF3 in the termination process involves not only stimulation of GTP hydrolysis by eRF3 on the ribosome and peptide release induced by eRF1, but also stimulation by eRF1 of guanine nucleotide binding to eRF3.

EXPERIMENTAL PROCEDURES

Chemicals—The fluorescent GDP/GTP derivatives mant-GDP and mant-GTP were from Jena Bioscience (Jena, Germany), a 100 mM GTP solution was from GE Biosciences (Piscataway, NJ) and a 100 mM GDP solution was from Roche Applied Science. Buffer A contained 20 mM Tris-HCl (pH 7.5), 100 mM potassium acetate, 2.5 mM $MgCl_2$, and 2 mM dithiothreitol.

Plasmids—Expression vectors for His_6-tagged eIFs 1, 1A, 4A, 4B, and 5 (20–22), and for eRF1, eRF1(NM) mutant (which corresponds to the N and M domains), and eRF3aC lacking the N-terminal 138 amino acids (12, 17, 23) as well as the MVHL-STOP transcription vector (17) have been described.

Purification of Factors and Ribosomal Subunits—Rabbit 40 S and 60 S subunits, eIFs 2, 3, 4F, and 5B, eEF1H and eEF2 were purified as described (20, 22, 24). His_6-tagged eIFs 1, 1A, 4A, 4B, and 5 were expressed in *Escherichia coli* BL21(DE3) and purified as described (20–22). Rabbit aminoacyl-tRNA synthetases were purified, and native total tRNA (Novagen) was aminoacylated with Met, Val, His, and [^{3}H]Leu as described (24). The specific activity of [^{3}H]Leu-tRNA^{Leu} was 160,000 cpm/pmol. His_6-tagged eRF1, eRF1(NM), and eRF3aC were expressed in *E. coli* BL21(DE3) and affinity-purified by chromatography on Ni^{2+}-NTA-agarose (Qiagen). After elution from Ni^{2+}-NTA-agarose, proteins were dialyzed overnight against buffer B (20 mM Tris HCl, pH 7.5, 100 mM KCl, 0.1 mM EDTA, 1 mM dithiothreitol, and 5% glycerol). eRF1 and eRF1(NM) were purified further by FPLC on a MonoQ HR5/5 column, from which they eluted at 250–270 mM KCl (buffer B). eRF3aC was further purified first by FPLC on a MonoQ HR5/5 column, from which it eluted at 250–270 mM KCl, and then by FPLC on a MonoS HR5/5 column, from which it eluted at 140–170 mM KCl. After all purification steps, proteins were dialyzed overnight against buffer B. The concentrations of factors were determined spectrophotometrically at 280 nm. Extinction coefficients were calculated from the amino acid composition of the proteins (25). The final preparation of eRF3 was free of guanine nucleotides as was determined by HPLC (26).

Gel Filtration— 400 pmol of eRF3aC and 2000 pmol of eRF1 were incubated in 200 μl of buffer A (with or without 2.5 mM $MgCl_2$) in the presence of 100 μM GTP or GDP, or in the absence of guanine nucleotides for 10 min at 37 °C. After incubation, reaction mixtures were loaded onto a FPLC Superdex 75 column equilibrated with buffer A, which either did not contain guanine nucleotides, or contained 100 μM GTP or GDP. Fractions that corresponded to peaks of optical density at 280 nm were loaded on to NuPAGE 4–12% Bis-Tris-Gel and after electrophoresis were stained with SimplyBlue/SafeStain (both Invitrogen).

Pretermination Complex Assembly and Peptide Release Assay—Pretermination complexes were assembled on MVHL-STOP mRNA in the presence of [^{3}H]Leu-tRNA^{Leu} essentially as described (17). 48 S complexes were assembled by incubating 3 μg of MHVL-STOP mRNA in a 400-μl reaction mixture containing buffer A supplemented with 1 mM ATP and 0.2 mM GTP, 150 μg of total tRNA (aminoacylated with Val, His, Met, and ^{3}H-labeled Leu), 30 pmol of 40 S subunits, 100 pmol of eIF2, 100 pmol of eIF3, 100 pmol of eIF4F, 120 pmol of eIF4A, 120 pmol of eIF4B, 300 pmol of eIF1, and 300 pmol of eIF1A for 15 min at 37 °C and then incubated for 15 min with 200 pmol of eIF5, 70 pmol of eIF5B, and 35 pmol of 60 S subunits to form 80 S initiation complexes. Pre-TCs were obtained by incubating 80 S complexes with 100 pmol of eEF1H and eEF2 for 15 min, and then purified by centrifugation in 10–30% sucrose density gradients prepared in buffer A. Fractions that corresponded to pre-TCs by optical density and the presence of [^{3}H]Leu were combined, diluted 3-fold with buffer A and used to assay peptide release. For this pre-TCs (0.15 pmol per 50 μl probe) were preincubated at 37 °C for 5 min with either 100 μM of unlabeled GTP or mant-GTP, or in the absence of guanine nucleotides, after which peptide release was initiated by addition of 1 pmol of eRF1 and eRF3aC. Peptide release was assayed using trichloroacetic acid precipitation (15).

Fluorescence Stopped-flow Kinetic Measurements—Fluorescence stopped-flow experiments were done using a SX-18MV spectrometer (Applied Photophysics, Leatherhead, UK). The fluorescence of mant-GTP, mant-GDP, and mant-dGTP was excited either directly at 349 nm or via FRET from tryptophan excited at 290 nm and was measured after passing a 400-nm cutoff filter (Schott, Duryea, PA). Experiments were performed

in buffer A (except when buffer A did not contain Mg^{2+}) at 25 °C by rapid mixing of equal volumes of reactants and monitoring the time course of the fluorescence change. In all experiments, after direct excitation at 349 nm, the fluorescence of mant-nucleotides increased within a range of 10–25%, whereas excitation at 290 nm via FRET resulted in 50–130% increase in fluorescence, depending on the nature of guanine nucleotide, and the concentrations of nucleotide and eRF3. Time courses shown represent the average of at least 7 individual transients. Primary analysis for the determination of k_{app} was done with the package provided by Applied Photophysics. Data were evaluated by fitting to exponential functions according to the following equations. For a single-exponential fit in Equation 1,

$$F(t) = F_\infty + A_1 e^{-k_{app}t} \quad \text{(Eq. 1)}$$

where F(*t*) is the fluorescence of time *t*, k_{app} and A are respectively the apparent rate constant and amplitude, and F_∞ is the final value of fluorescence. The values of the association (k_{+1}) and dissociation (k_{-1}) rate constants, and the standard deviations were estimated from the slope and Y-axis intercept, respectively, of the linear concentration dependence of k_{app}. For a double-exponential fit, the time courses were evaluated according to Equation 2,

$$F(t) = F_\infty + A_1 e^{-k_{app1}t} + A_2 e^{-k_{app2}t} \quad \text{(Eq. 2)}$$

where F(*t*) is the fluorescence at time *t*, k_{app1} and k_{app2} and A_1 and A_2, respectively, are the apparent rate constants and amplitudes for the first and the second components, and F_∞ represents the final fluorescence. The values of the individual rate constants, k_1, k_{-1}, k_2, and k_{-2}, were calculated from k_{app1} and k_{app2} either analytically by building the sum and the product of k_{app} and plotting their concentration dependences, as described (27), or by global fitting using Scientist software (MicroMath). The reported values of the rate constants are the averages of values obtained by the two calculation methods. The standard deviations represent ranges of maximum deviation for a given constant from either the standard deviation of the analytical solution or the statistics of global fitting.

Steady State Fluorescence Measurements and Chase Titration—Fluorescence emission spectra were recorded on a Fluoromax-3 spectrophotometer (Jobin Yvon Inc., Edison, NJ) in a 10 × 10 mm (i.d.) quartz cuvette (Bel-Art products, Pequannock, NJ) at 25 ± 1 °C. All measurements were done in buffer A with or without 2.5 mM Mg^{2+}.

Binding of mant-GTP to eRF3aC was monitored using an excitation wavelength of 290 nm and an emission wavelength of 350 nm. To estimate the equilibrium dissociation constant, K_d, of the mant-GTP·eRF3 complex, the fluorescence of 0.5 μM eRF3aC was measured alone and in the presence of increasing amounts of mant-GTP. Binding of mant-GTP to eRF3aC·eRF1 was monitored using an excitation wavelength of 290 nm and an emission wavelength of 440 nm. To estimate the equilibrium dissociation constant, K_d, of the mant-GTP·eRF3·eRF1 complex, the fluorescence of mant-GTP (increasing amounts) was measured alone and in the presence of 0.1 μM eRF3 and 2 μM eRF1. Dilution was less than 2% in all cases. For analysis of the titration data, the one-site binding model in Equation 3 was used,

$$Y = Y_{max} \times X/(K_d + X) \quad \text{(Eq. 3)}$$

where X is the concentration of mant-GTP in the reaction, Y is the difference in the fluorescence intensities either of eRF3aC in the presence and absence of mant-GTP (FRET) or of mant-GTP in the presence and absence of eRF3aC·eRF1. Y_{max} is the maximum value of FRET. Data were evaluated using GraphPad Prism 4 (GraphPad Software, Inc., San Diego, CA).

The equilibrium dissociation constants of the unmodified guanine nucleotides were determined by chase titration of mant-guanine nucleotides from their complexes either with eRF3aC alone or with eRF3aC·eRF1, by increasing concentrations of unmodified nucleotides. The chase of mant-guanine nucleotides was monitored by the change in fluorescence of the mant- group after excitation at 349 or 297 nm. The chase of mant-GTP from eRF3aC by GTP was measured using 0.8 μM eRF3aC, 3 μM mant-GTP, and increasing concentrations of unlabeled GTP. The chase of mant-GTP from eRF3aC·eRF1 by GTP was measured using 0.8 μM eRF3aC, 8 μM eRF1, 3 μM mant-GTP, and increasing concentrations of unlabeled GTP. The chase of mant-GDP by GDP from eRF3aC in the presence of 2.5 mM Mg^{2+} was measured using 0.3 μM eRF3aC, 3 μM mant-GDP, and increasing concentrations of unlabeled GDP. The chase of mant-GDP by GDP from eRF3aC in the absence of Mg^{2+} was measured using 0.8 μM eRF3aC, 8 μM mant-GDP, and increasing concentrations of unlabeled GDP. The chase of mant-GTP by GDP from eRF3aC·eRF1 in the presence of 2.5 mM Mg^{2+} was measured using 0.8 μM eRF3aC, 8 μM eRF1, 3 μM mant-GTP, and increasing concentrations of unlabeled GDP. The chase of mant-GDP by GDP from eRF3aC·eRF1 in the absence of Mg^{2+} was measured using 0.8 μM eRF3aC, 8 μM eRF1, 3 μM mant-GDP, and increasing concentrations of unlabeled GDP. For analyzing the chase titration data, the following model in Equations 4 and 5 were used,

$$P + A \overset{K_A}{\longleftrightarrow} PA \quad \text{(Eq. 4)}$$

$$P + I \overset{K_I}{\longleftrightarrow} PI \quad \text{(Eq. 5)}$$

where P is eRF3aC or the eRF3aC·eRF1 complex; A is mant-GTP or mant-GDP; I is GTP or GDP; K_A and K_I are equilibrium dissociation constants of A and I, respectively. In this case the fluorescence of a mant-guanine nucleotide observed in the presence of a competitor unlabeled guanine nucleotide, F(I), can be described by the following Equation 6,

$$F(I) = F_{max} \times [A]/([A] + K_A(1 + [I]/K_I)) + F_{min} \quad \text{(Eq. 6)}$$

where F_{max} and F_{min} represent fluorescence intensities of PA and A, respectively. The equilibrium dissociation constant of unmodified guanine nucleotide, K_I, was calculated by fitting the above equation to the titration data using GraphPad Prism 4.

GTP Hydrolysis—To measure eRF1- and ribosome-dependent multiple turnover GTP hydrolysis by eRF3, 0.4 μM eRF3, 1.4 μM eRF1, and 80 S ribosomes (increasing concentrations from 0.1 to 2 μM) were preincubated in buffer A at 25 °C, and hydrolysis was started by adding 10 μM [γ-^{32}P]GTP. Aliquots (10 μl) were taken at the indicated times and manually quenched with 50 mM H_2SO_4/2 mM KH_2PO_4. [γ-^{32}P]P_i release was analyzed by ammonium phosphomolybdate extraction. Measurements of GTP hydrolysis after periods of less than 1 min were performed using a quench-flow apparatus (KinTek, Austin, TX). Samples were quenched and analyzed as described above. Blank values resulting from the presence of 3.2% P_i in [γ-^{32}P]GTP preparations were determined in the absence of eRF3 and subtracted from all measurements.

RESULTS

Fluorescence Changes of mant-GTP/mant-GDP upon Binding to eRF3—The fluorescent GDP and GTP derivatives mant-GDP and mant-GTP contain a mant group attached to the ribose moiety and have been widely used to study nucleotide binding by proteins. To investigate guanine nucleotide binding to eRF3, we used recombinant human eRF3aC lacking the N-terminal 138 amino acids, which are dispensable for the eRF3 GTPase activity and for its stimulation of eRF1 release activity (12). This polypeptide is referred to as eRF3 below. Fluorescence changes of the mant-nucleotide upon its binding to a protein can be monitored either upon direct excitation of the fluorophore or indirect excitation via FRET, in which tryptophan residues close to the nucleotide binding site serve as fluorescence donors and the mant-labeled nucleotide as acceptor (28, 29). Upon direct excitation at 349 nm, the fluorescence of both mant-GTP and mant-GDP increased upon binding to eRF3 without a significant shift in the emission maximum (440 nm) (Fig. 1, *A* and *B*). Upon excitation at 290 nm, substantial energy transfer occurred between tryptophan residues of eRF3 and the mant-groups in both eRF3·mant-GTP and eRF3·mant-GDP complexes, manifested as a simultaneous decrease in tryptophan fluorescence and an increase in mant fluorescence compared with the protein alone and free mant-nucleotides, respectively (Fig. 1, *C* and *D*). The G domain of eRF3 contains four tryptophan residues within 25 Å of the nucleotide binding site (Trp^{250} and Trp^{254} in the switch I region, Trp^{358} and Trp^{407}; Fig. 1*E*), which are all close enough to contribute to FRET.

Mant-GTP was fully active in translation termination. Thus, eRF1-mediated peptide release from pretermination complexes assembled on a derivative of β-globin mRNA encoding a MVHL tetrapeptide followed by a UAA termination codon was stimulated equally by eRF3·mant-GTP and eRF3·GTP (Fig. 1*F*).

Association of eRF3 with eRF1— eRF3 and eRF1 form a stable complex by interaction of their C-terminal domains (8, 12, 13). The cooperation between eRF1 and eRF3 in accelerating peptidyl-tRNA hydrolysis and the stimulation of eRF3 ribosome-dependent GTPase activity by eRF1 both require the eRF3-binding C-terminal domain (CTD) of eRF1 (5, 11, 17). To investigate the potential influence of eRF1 on the kinetics of binding of guanine nucleotides to eRF3, we first studied the interaction between eRF1 and eRF3 in the presence or absence of GTP or GDP using gel filtration on Superdex 75. The concentrations of eRF3, eRF1, and guanine nucleotides were 2, 10, and 100 μM, respectively. During gel filtration, samples are usually diluted about 5-fold, and the concentrations of eRF3 and eRF1 in the eluate were therefore reduced to ~0.4 and 2 μM, respectively. Guanine nucleotides were present in gel filtration buffers at a constant concentration throughout the procedure. At the eRF1 and eRF3 concentrations used in the gel filtration assay, the majority of eRF3 was associated with eRF1 independent of the nucleotide (Fig. 1*G*). Similar results were obtained in the absence of Mg^{2+} (data not shown). To ensure that the majority of eRF3 formed a complex with eRF1 in the kinetic experiments described below, factors were used at concentrations above those used during gel filtration.

Kinetics of Interaction of eRF3 with GDP—The kinetics of binding of mant-GDP to eRF3 was measured by fluorescence stopped flow (Fig. 2, *A–C*). Both approaches, *i.e.* excitation of the mant-group either directly, or by FRET from tryptophan residues, gave identical values for the rate constants in all cases studied. Kinetics was measured under pseudo-first-order conditions at 0.5 μM eRF3, and concentrations of mant-GDP from 1.5 to 5 μM. Time courses (Fig. 2*A* and data not shown) could be fitted by a single-exponential term, yielding pseudo-first-order rate constants, k_{app}, which depended linearly on the mant-GDP concentration (Fig. 2*C* and data not shown). This behavior is consistent with a one-step binding model in Equation 7.

$$\text{eRF3} + \text{mant-GDP} \underset{k_{-1}}{\overset{k_{+1}}{\longleftrightarrow}} \text{eRF3·mant-GDP} \qquad \text{(Eq. 7)}$$

Association and dissociation rate constants k_{+1} and k_{-1} can be determined from the linear concentration dependence of k_{app} using Equation 8.

$$k_{app} = k_{+1}[\text{mant-GDP}] + k_{-1} \qquad \text{(Eq. 8)}$$

The slope of the straight line fitted to the data points defines the association rate constant, k_{+1} ($M^{-1}\ s^{-1}$), and the intercept with the *y*-axis yields the dissociation rate constant, k_{-1} (s^{-1}). The value of k_{-1} was also determined more accurately in a displacement experiment in which a 50-fold molar excess of unlabeled GDP was used to displace mant-GDP from its complex with eRF3. The time courses of mant-GDP dissociation from the binary complex indicated by a decrease in the fluorescence signal (Fig. 2*B* and data not shown) were also fitted by a single-exponential term yielding the dissociation rate constants k_{-1}. From the concentration dependence of k_{app}, the values were $k_{+1} = 3.1\ \mu M^{-1}\ s^{-1}$ and $k_{-1} = 2.4\ s^{-1}$, for the association and dissociation rate constants, respectively, yielding a value of ~0.8 μM for the equilibrium dissociation constant, K_d (Table 1 and Fig. 7*A*).

To investigate the potential influence of eRF1 on the interaction of mant-GDP with eRF3, eRF3 was preincubated with a 10-fold molar excess of eRF1 to form the eRF3·eRF1 complex. Time courses of the binding of mant-GDP to eRF3·eRF1 were measured by monitoring mant fluorescence upon direct excitation (data not shown) or FRET (Fig. 2, *D–F*) as above. The apparent rate constants of binding were linearly dependent on

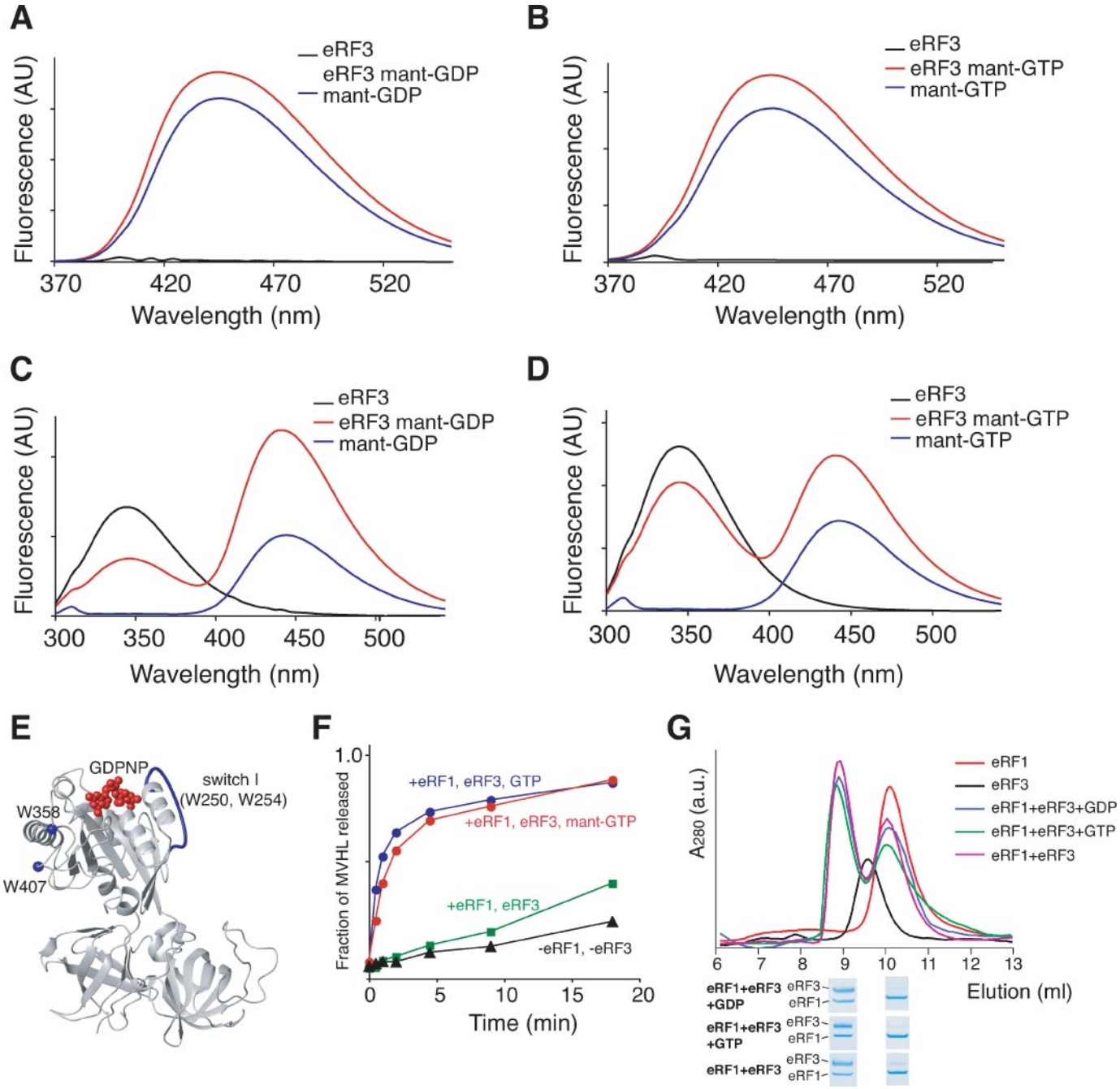

FIGURE 1. **Formation of eRF3 complexes with mant-GDP/mant-GTP and eRF1.** *A*, emission spectra of mant-GDP (3 μM) in the absence (*blue*) and in the presence of eRF3 (0.4 μM) (*red*) upon excitation at 349 nm; emission spectrum of eRF3 (0.4 μM) (*black*) at the same excitation wavelength. *B*, same as in *A* with mant-GTP. *C*, emission spectra of eRF3 (0.4 μM) (*black*) and mant-GDP (3 μM) in the absence (*blue*) and in the presence of eRF3 (0.4 μM) (*red*) upon excitation at 290 nm (FRET). *D*, same as in *C* with mant-GTP. *E*, *ribbon diagram* of yeast eRF3 (18) (*gray*) with bound GMPPNP (*red*). *Blue spheres* represent the positions of Trp^{358} and Trp^{407} of human eRF3 mapped onto the crystal structure of yeast eRF3; the unstructured switch I region that in human eRF3 contains Trp^{250} and Trp^{254} is also colored *blue*. *F*, kinetics of [^{3}H]MVHL peptide release from pre-TCs in the presence of eRF1 and eRF3 (*green squares*), eRF1, eRF3, and GTP (*blue circles*), eRF1, eRF3, and mant-GTP (*red circles*), and in the absence of eRFs (*black triangles*). *G*, elution profiles from Superdex 75 of eRF1 (*red*), eRF3 (*black*), eRF1, and eRF3 incubated in the presence of 100 μM GTP (*green*) or GDP (*blue*), or in the absence of guanine nucleotides (*magenta*). The stained SDS-PAAG panels show the presence of eRF1 and eRF3 in the corresponding elution peaks as indicated.

the mant-GDP concentration (Fig. 2*F* and data not shown). The values of k_{-1} were determined in displacement experiments (Fig. 2*E* and data not shown). The association and dissociation rate constants (Table 1 and Fig. 7*A*) determined from the linear plots and the calculated $K_d = 1.1$ μM for the complex of mant-GDP with eRF3·eRF1 were very similar to those obtained for binding of mant-GDP to eRF3 alone (Table 1 and Fig. 7*A*).

To examine whether 80 S ribosomes influenced the binding of mant-GDP to the eRF3·eRF1 complex, eRF3 was first preincubated with eRF1 and 80 S ribosomes in the ratio 1:3.5:3.75. The concentration of ribosomes used in this experiment was saturating at least for the eRF1·eRF3·GTP complex, as will be shown in the next section (Fig. 4*G*). The kinetics of mant-GDP binding to the complex was monitored by mant-GDP fluores-

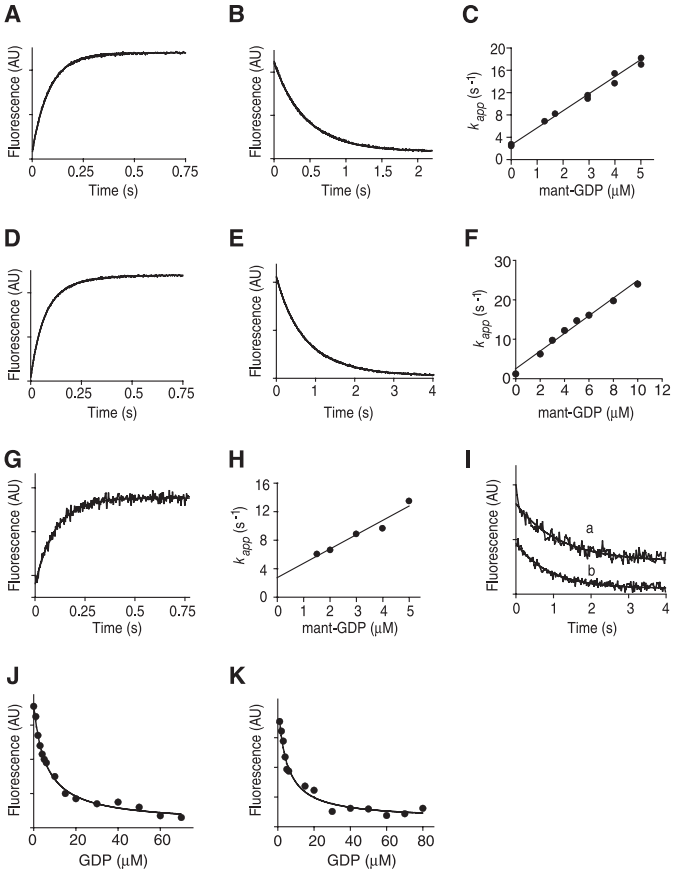

FIGURE 2. **Binding of GDP and mant-GDP to eRF3 alone, to eRF3 and eRF1, and to eRF3, eRF1 and 80 S ribosomes at 2.5 mM Mg^{2+}.** *A*, time course of the association of mant-GDP (3 μM) with eRF3 (0.5 μM). *B*, dissociation of the mant-GDP·eRF3 complex (0.5 μM eRF3 and 3 μM mant-GDP) in the presence of GDP (150 μM). The *smooth lines* represent single-exponential fits that yielded the respective rate constants k_{app}. *C*, concentration dependence of k_{app} values for eRF3/mant-GDP association. *D*, time course of the association of mant-GDP (3 μM) with eRF3 (0.5 μM) in the presence of eRF1 (5 μM). *E*, dissociation of the mant-GDP·eRF3·eRF1 complex (0.5 μM eRF3, 5 μM eRF1, and 3 μM mant-GDP) in the presence of GDP (150 μM). *F*, concentration dependence of k_{app} values for eRF3/mant-GDP association in the presence of eRF1. *G*, time course of the association of mant-GDP (4 μM) with eRF3 (0.4 μM) in the presence of eRF1 (1.4 μM) and 80 S ribosomes (1.5 μM). *H*, concentration dependence of k_{app} values for eRF3/mant-GDP association in the presence of eRF1 and 80 S ribosomes. *I*, time courses of dissociation of the mant-GDP·eRF3·eRF1 complex (0.4 μM eRF3, 1.4 μM eRF1, and 5 μM mant-GDP) in the presence of GTP alone (250 μM) (*curve a*) or in the presence of GTP (250 μM) and 80 S ribosomes (1.5 μM) (*curve b*). Mant fluorescence was excited either by FRET at 290 nm (*A*, *B*, *D*, *E*) or directly at 349 nm (*G* and *I*). *J* and *K*, chase titration of eRF3·mant-GDP (0.4 μM eRF3 and 3 μM mant-GDP) and eRF1·eRF3·mant-GTP (0.8 μM eRF3, 8 μM eRF1, and 3 μM mant-GTP) complexes, respectively, with GDP. *Solid lines* represent the results of the fits, as described under "Experimental Procedures."

cence upon direct excitation (Fig. 2*G*). The association and dissociation rate constants (Table 1 and Fig. 7*A*), determined from the linear plot (Fig. 2*H*), and the calculated constant K_d value (~1 μM) for binding of mant-GDP to the eRF3·eRF1·80S complex were very similar to those obtained for binding of mant-GDP both to eRF3 alone and to the eRF3·eRF1 complex (Table 1 and Fig. 7*A*). In direct displacement experiments, the presence of 80 S ribosomes did not influence the dissociation rate of mant-GDP from its complex with eRF3·eRF1 (Fig. 2*I*, *curves a* and *b*).

The K_d values of 1.3 and 1.1 μM for binding of unlabeled GDP to eRF3 alone and to the eRF3·eRF1 complex, respectively (Table 2), were determined by titrating eRF3·mant-GDP and eRF3·eRF1·mant-GTP complexes with unlabeled GDP (Fig. 2, *J* and *K*) and were very similar to the values for its mant- derivative (Table 1).

These results indicate that eRF1 does not influence binding of GDP to eRF3, and that the addition of 80 S ribosomes under conditions when the majority of eRF3 was bound to eRF1 also did not influence the binding affinity of GDP to eRF3 or the exchange of GDP by GTP on the eRF3·eRF1 complex.

Kinetics of Interaction of eRF3 with GTP—The kinetics of binding of mant-GTP to eRF3 was monitored by FRET at 0.5 μM eRF3, with the concentration of mant-GTP varying from 2 to 25 μM (Fig. 3, *A–C*). In contrast to mant-GDP binding to eRF3, fitting of the stopped-flow traces required two exponential terms (Fig. 3*A*). The apparent rate constants of the fast step were increasing linearly with the mant-GTP concentration, while the rate of the slow step was practically unchanged. A two-exponential time course could reflect either a two-step binding pathway or simply heterogeneity of mant-GTP or of the protein preparation. The biphasic kinetics was not a consequence of presence of mant-GDP in the mant-GTP preparation, because we did not detect any mant-GDP in mant-GTP preparations using TLC or HPLC (26, 30) (data not shown), and because the investigation of mant-GTP and eRF3 binding in the presence of an energy pump (phosphoenolpyruvate and pyruvate kinase) did not yield a single-exponential curve. Mant-GTP is a mixture of the 2′ and 3′ isomers present in an ~1:1 ratio (producer's information); however, double exponential kinetics could not be explained by isomerization of the mant-group from 2′ to 3′ positions of the ribose moiety and subsequent preferential binding of eRF3 to one isomer either, because double exponential transients were also observed using

TABLE 1

Rate constants and equilibrium dissociation constants of the interaction between mant-guanine nucleotides and eRF3 alone or its complexes with eRF1 and 80 S ribosomes determined by fluorescence stopped-flow

Complex	Nucleotide	k_{+1}	k_{-1}	k_{+2}	k_{-2}	K_d
		$\mu M^{-1}\,s^{-1}$	s^{-1}	s^{-1}	s^{-1}	μM
eRF3	mant-GDP	3.1 ± 0.1	2.4 ± 0.2			0.8 ± 0.1
eRF3·eRF1	mant-GDP	2.2 ± 0.1	2.4 ± 0.6			1.1 ± 0.3
eRF3·eRF1·80S	mant-GDP	2.3 ± 0.2	2.3 ± 1.1			1 ± 0.5
eRF3	mant-GTP	0.7 ± 0.1	13 ± 1	2.5 ± 0.2	3.3 ± 1	23 ± 3 (11 ± 4[a])
eRF3·eRF1	mant-GTP	0.50 ± 0.03	0.14 ± 0.03			0.3 ± 0.1 (0.3 ± 0.1[a])
eRF3·eRF1·80S	mant-GTP	0.27 ± 0.03	0.17 ± 0.13			0.6 ± 0.2
eRF3 (−Mg^{2+})	mant-GDP	6.7 ± 0.2	1.4 ± 0.6			0.2 ± 0.1
eRF3·eRF1 (−Mg^{2+})	mant-GDP	7.6 ± 0.3	2.8 ± 1.3			0.4 ± 0.2
eRF3 (−Mg^{2+})	mant-GTP	3.1 ± 0.2	27 ± 3	3.8 ± 0.3	3 ± 1	7 ± 2 (6 ± 0.1[a])
eRF3·eRF1 (−Mg^{2+})	mant-GTP	3.5 ± 0.4	13 ± 1	2.5 ± 0.3	1.7 ± 0.5	2.4 ± 0.9 (1.6 ± 0.2[a])

[a] Determined at equilibrium by fluorescence titration.

TABLE 2

Equilibrium dissociation constants of the interaction between guanine nucleotides and eRF3 alone or its complex with eRF1

Complex	Nucleotide	K_d	K_d-Mg^{2+}
		μM	μM
eRF3	GDP	1.3 ± 0.1	0.13 ± 0.01
eRF3·eRF1	GDP	1.1 ± 0.1	0.45 ± 0.1
eRF3	GTP	69 ± 7	47 ± 5
eRF3·eRF1	GTP	0.7 ± 0.2	25 ± 3

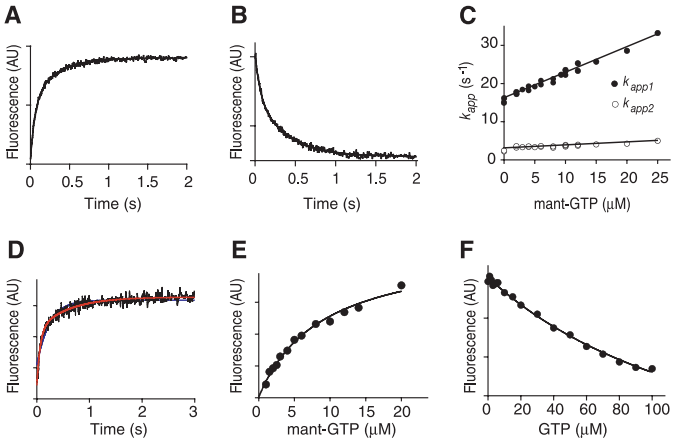

FIGURE 3. **Binding of GTP and mant-GTP to eRF3 at 2.5 mM Mg^{2+}.** *A*, time course of the association of mant-GTP (4 μM) with eRF3 (0.5 μM). *B*, dissociation of the mant-GTP·eRF3 complex (0.5 μM eRF3 and 4 μM mant-GTP) in the presence of GTP (200 μM). The *smooth lines* represent double-exponential fits to the data that yielded the respective rate constants k_{app1} and k_{app2} for the first and second steps, respectively. *C*, concentration dependence of k_{app1} and k_{app2}. *Smooth lines* represent theoretical curves for the first (*filled circles*) and second (*open circles*) step generated using the values of the elemental rate constants in Table 1. *D*, time course of the association of mant-dGTP (4 μM) with eRF3 (0.5 μM). The *smooth red* and *blue lines* represent double-exponential and single-exponential fits, respectively. Mant fluorescence was excited either by FRET at 290 nm (*A* and *B*) or directly at 349 nm (*D*). *E*, titration of eRF3 (0.5 μM) with mant-GTP. The *solid line* shows the fit to the data using a one-site binding model. *F*, chase titration of the eRF3·mant-GTP complex (0.8 μM eRF3 and 3 μM mant-GTP) with GTP. *Solid line* represents the result of the fit, as described under "Experimental Procedures."

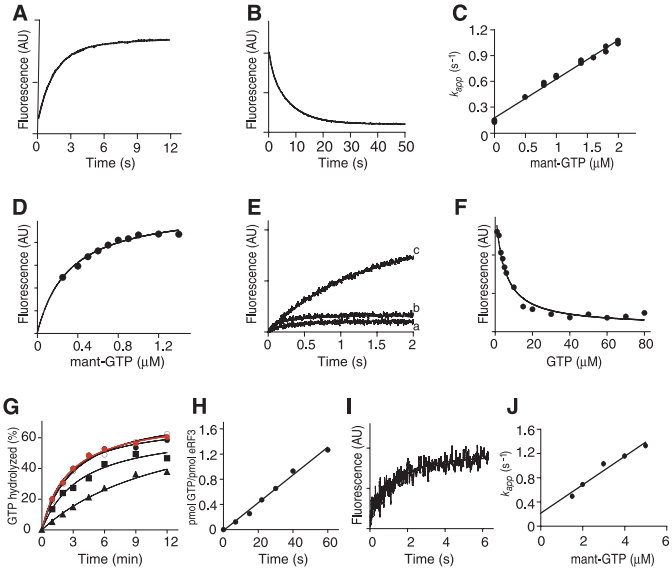

FIGURE 4. **Binding of GTP and mant-GTP to eRF3 in the presence of eRF1 or eRF1 and 80 S ribosomes at 2.5 mM Mg^{2+}.** *A*, time course of the association of mant-GTP (1 μM) with eRF3 (0.25 μM) in the presence of eRF1 (5 μM). *B*, dissociation of the mant-GTP·eRF3·eRF1 complex (0.25 μM eRF3, 5 μM eRF1, and 1 μM mant-GTP) in the presence of GTP (50 μM). The *smooth lines* represent exponential fits that yielded the respective rate constants k_{app}. *C*, concentration dependence of k_{app}. *D*, titration of the eRF3·eRF1 complex (0.1 μM eRF3 and 2 μM eRF1) with mant-GTP. The *solid line* shows the fit to the data using a one-site binding model. *E*, time courses of the association of mant-GTP (0.8 μM) with eRF3 (0.25 μM) (*curve a*), with eRF3 in the presence of eRF1(NM) (0.75 μM) (*curve b*), and with eRF3 in the presence of eRF1 (0.75 μM) (*curve c*). *F*, chase titration of the eRF1·eRF3·mant-GTP complex (0.8 μM eRF3, 8 μM eRF1, and 3 μM mant-GTP) with GTP. *Solid line* represents the result of the fit, as described under "Experimental Procedures." *G*, time courses of multiple turnover hydrolysis of GTP (10 μM) in the presence of 0.4 μM eRF3, 1.4 μM eRF1, and increasing concentrations of 80 S ribosomes (0.1 μM, *black triangles*; 0.4 μM, *black squares*; 1 μM, *black closed circles*; 1.5 μM, *red closed circles*; and 2 μM, *black open circles*). *H*, time course of hydrolysis of GTP (10 μM) in the presence of 0.4 μM eRF3, 1.4 μM eRF1, and 1.5 μM 80 S ribosomes shown as pmol of GTP hydrolyzed by 1 pmol of eRF3. *I*, time course of the association of mant-GTP (4 μM) with eRF3 (0.4 μM) in the presence of eRF1 (1.4 μM) and 80 S ribosomes (1.5 μM). The smooth line represents a single-exponential fit. *J*, concentration dependence of k_{app}. Mant fluorescence was excited either by FRET at 290 nm (*A*, *B*, and *E*) or directly at 349 nm (*I*).

mant-dGTP, which is unable to undergo isomerization (Fig. 3*D*). Heterogeneity of eRF3 is unlikely because biphasic kinetics was not observed in the experiments with mant-GDP, and because the same results with mant-GTP were obtained with different eRF3 preparations. A two-step binding mechanism involving isomerization of eRF3 prior to binding of mant-GTP is also unlikely because it would be expected to cause two-exponential time courses for binding of mant-GDP as well, which was not observed. The double exponential transients therefore most likely reflect a two-step binding mechanism (which is not uncommon for nucleotide-binding proteins) in which an initial complex formed between eRF3 and mant-GTP undergoes subsequent conformational change in Equation 9.

$$\text{eRF3} + \text{mant-GTP} \underset{k_{-1}}{\overset{k_{+1}}{\longleftrightarrow}} \text{eRF3·mant-GTP} \underset{k_{-2}}{\overset{k_{+2}}{\longleftrightarrow}} \text{eRF3·mant-GTP} \quad \text{(Eq. 9)}$$

In a displacement experiment (Fig. 3*B*), the dissociation of mant-GTP was also biphasic. By calculation (see "Experimental Procedures"), the association rate constant for the first step was $k_{+1} = 0.7\ \mu M^{-1}\ s^{-1}$, the rate constant of the following rearrangement was $k_{+2} = 2.5\ s^{-1}$, and the dissociation rate constants k_{-1} and k_{-2} were 13 and 3.3 s^{-1}, respectively (Table 1 and Fig. 7*A*). The resulting calculated K_d value of 23 μM (Table 1) agreed well with the K_d value obtained by equilibrium titration (Fig. 3*E* and Table 1). The K_d value of 69 μM for binding of unlabeled GTP to eRF3 (Table 2) was estimated by titrating the eRF3·mant-GTP complex with unlabeled GTP (Fig. 3*F*). In conclusion, these data indicate that the affinity of eRF3 for GTP is more than one order of magnitude lower than for GDP, and that mant-GTP dissociates from eRF3 at least as rapidly as mant-GDP, because the slowest step for mant-GTP dissociation has a rate constant of 3.3 s^{-1}, which is very similar to the dissociation rate constant observed with mant-GDP, 2.4 s^{-1}.

To examine whether eRF1 influenced the binding of mant-GTP to eRF3, eRF3 was preincubated with a 20-fold excess of eRF1 to form the eRF3·eRF1 complex. The time courses for mant-GTP association (Fig. 4*A*) and dissociation (Fig. 4*B*) showed a dominant step, the k_{app} of which depended linearly on the mant-GTP concentration (Fig. 4*C*). The association and dissociation rate constants (0.5 $\mu M^{-1}\ s^{-1}$ and 0.14 s^{-1}, respec-

tively) yielded a K_d value of 0.3 μM (Table 1 and Fig. 7*A*), which was identical to the K_d value obtained by equilibrium titration (Fig. 4*D* and Table 1). Thus, in contrast to the binding of mant-GDP to eRF3, which was not influenced by eRF1, the association of eRF3 with eRF1 stabilized the binding of mant-GTP to eRF3 by more than one order of magnitude. The stabilizing effect was mostly due to lowering the dissociation rate constant, from 3.3 s^{-1} in the absence of eRF1 to 0.14 s^{-1} in its presence. The effect of eRF1 was specific, because the eRF1(NM) truncation mutant that lacks the eRF3-binding CTD did not influence binding of mant-GTP to eRF3, and as shown in Fig. 4*E*, the stopped-flow traces for mant-GTP and eRF3 in the absence of eRF1 (*curve a*) and in the presence of eRF1(NM) (*curve b*) were similar and both differed strongly from the trace observed in the presence of full-length eRF1 (*curve c*). The K_d value of 0.7 μM for binding of unlabeled GTP to the eRF3·eRF1 complex (Table 2) was determined by titrating the eRF3·eRF1·mant-GTP complex with unlabeled GTP (Fig. 4*F*) and was very similar to that for its mant-derivative (Table 1).

To examine whether ribosomes influence the binding of mant-GTP to eRF3·eRF1, eRF3 was first preincubated with eRF1 and 80 S ribosomes. To verify that the concentration of 80 S ribosomes was saturating, the time courses of multiple turnover GTP hydrolysis at fixed concentrations of eRF3 and eRF1 that were used for the mant-GTP binding assay and increasing concentrations of 80 S ribosomes were measured (Fig. 4*G*). The results of GTP hydrolysis confirmed that the concentration of 80 S ribosomes of 1.5 μM used in the mant-GTP binding assay was saturating for the eRF1·eRF3·GTP complex. The K_d values for binding of eRF1 and eRF3 individually to 80 S ribosomes have been estimated as 1.8 μM and 2.3 μM, respectively (19). The observation reported here that saturation was reached at 1.5 μM 80 S ribosomes suggests that the affinity of the eRF1·eRF3·GTP complex to 80 S ribosomes is higher than of the individual factors. Although it would be preferable to investigate the influence of ribosomes on binding of GTP to eRF3 using the non-hydrolyzable or slowly hydrolyzable GTP analogs mant-GMPPNP or mant-GTP-γS, neither of them behaved like mant-GTP in binding to eRF3 or to eRF3·eRF1: the affinity to eRF3 of mant-GMPPNP was lower, and the affinity of mant-GTP-γS was noticeably higher than that of mant-GTP (data not shown). However, consistent with prior data (16), GTP hydrolysis by eRF3 was slow (Fig. 4*H*) and over the time interval of the stopped-flow experiments (~6 s) constituted ~0.1 pmol of GTP per 1 pmol of eRF3. Consistently, kinetic traces obtained with mant-GTP did not show behavior that could be associated with GTP hydrolysis. The kinetics of mant-GTP binding was monitored by the fluorescence of mant-GTP upon direct excitation (Fig. 4*I*). The stopped-flow traces could be fitted by a single-exponential term, and the apparent rate constants were linearly dependent on the mant-GTP concentration (Fig. 4*J*). The association and dissociation rate constants (0.27 $\mu M^{-1}\,s^{-1}$ and 0.17 s^{-1}, respectively), determined from the linear plot, yielded the calculated $K_d = 0.6$ μM (Table 1 and Fig. 7*A*) for binding of mant-GTP to the eRF3·eRF1·80S complex, which was very similar to the value for the binding of mant-GTP to eRF3·eRF1 (Table 1). These results indicate that eRF1 strongly increases the affinity of GTP to eRF3, whereas 80 S ribosomes do not appreciably influence the binding of GTP to eRF3·eRF1.

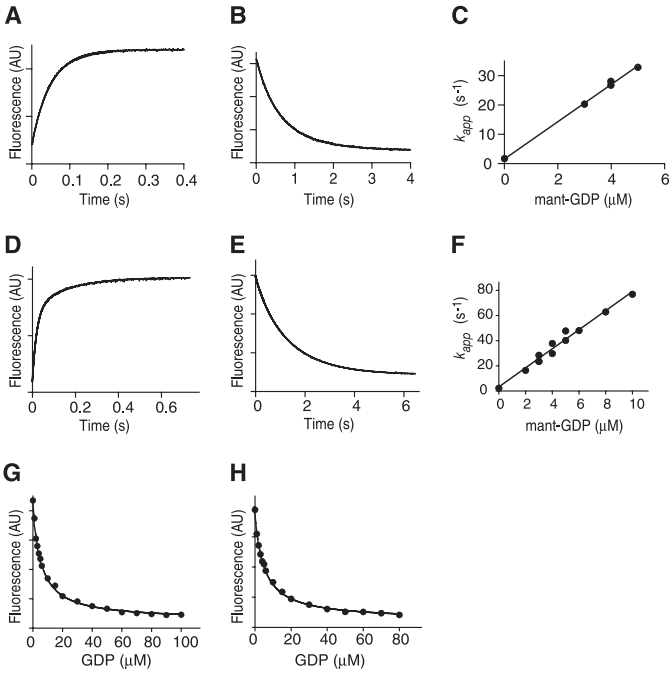

FIGURE 5. **Binding of GDP and mant-GDP to eRF3 alone, and to eRF3 and eRF1 in the absence of Mg^{2+}.** *A*, time course of the association of mant-GDP (3 μM) with eRF3 (0.5 μM). *B*, dissociation of mant-GDP·eRF3 complex (0.5 μM eRF3 and 3 μM mant-GDP) in the presence of GDP (150 μM). The *smooth lines* represent single-exponential fits. *C*, concentration dependence of k_{app} for mant-GDP-eRF3 association. *D*, time course of the association of mant-GDP (5 μM) and 0.5 μM eRF3 in the presence of eRF1 (5 μM). *E*, dissociation of the mant-GDP·eRF3·eRF1 complex (0.5 μM eRF3, 5 μM eRF1, 3 μM mant-GDP) in the presence of GDP (150 μM). *F*, concentration dependence of k_{app} for mant-GDP-eRF3 association in the presence of eRF1. *G* and *H*, chase titration of eRF3·mant-GDP (0.8 μM eRF3 and 3 μM mant-GDP) and eRF1·eRF3·mant-GDP (0.8 μM eRF3, 8 μM eRF1 and 3 μM mant-GDP) complexes, respectively, with GDP. *Solid lines* represent the results of the fits, as described under "Experimental Procedures."

Influence of Mg^{2+} on Guanine Nucleotide Binding to eRF3—Whereas GTP is usually bound to G proteins in a complex with Mg^{2+}, and Mg^{2+} contributes to the stability of GTP binding to many G proteins, the requirement for Mg^{2+} to support binding of GDP varies among G proteins (31). Although a Mg^{2+} ion was not found in eRF3 crystals into which GDP or GDPNP had been soaked (18), we nevertheless examined the contribution of Mg^{2+} to the affinity of eRF3 for GDP and GTP by measuring the binding of mant-GTP/GDP and unlabeled GTP/GDP to eRF3 and to eRF3·eRF1 in the absence of Mg^{2+} and compared the results with data from the experiments described above, which were done in the presence of 2.5 mM Mg^{2+}. In all kinetic experiments, time courses were monitored by mant fluorescence excited by FRET from tryptophan residues of eRF3.

In the case of mant-GDP and eRF3, the stopped-flow traces could be fitted by a single-exponential term (Fig. 5, *A* and *B*), yielding the k_{app} values linearly increasing with mant-GDP concentrations (Fig. 5*C*). The association and dissociation rate constants (6.7 $\mu M^{-1}\,s^{-1}$ and 1.4 s^{-1}, respectively) and the calculated K_d value (0.2 μM; Table 1 and Fig. 7*B*) indicate that in the absence of Mg^{2+} the affinity of mant-GDP to eRF3 is increased about 4-fold because of both a small increase in the association rate constant and a decrease in the dissociation rate constant.

The $K_d = 0.13$ μM for binding of unlabeled GDP to eRF3 (Table 2) was determined by titrating the eRF3·mant-GDP complex with unlabeled GDP (Fig. 5*G*) and was very similar to that for its mant-derivative (Table 1). In the case of mant-GDP and the eRF3·eRF1 complex, the stopped-flow traces could also be fitted by a single-exponential term (Fig. 5, *D–F*). The calculated $K_d = 0.4$ μM (Table 1) indicated that as in the case of eRF3 alone, the absence of Mg^{2+} ions slightly increased the affinity of mant-GDP to eRF3·eRF1, this time due to a slight increase in the association rate constant $k_{+1} = 7.6\ \mu M^{-1}\ s^{-1}$ (Table 1 and Fig. 7*B*). The $K_d = 0.45$ μM for binding of unlabeled GDP to the eRF3·eRF1 complex (Table 2) was determined by titrating the eRF3·eRF1·mant-GDP complex with unlabeled GDP (Fig. 5*H*) and again was very similar to that for its mant-derivative (Table 1).

In the absence of Mg^{2+} ions, the stopped-flow traces for mant-GTP association/dissociation with/from eRF3 alone (Fig. 6, *A* and *B*) or eRF3·eRF1 (Fig. 6, *F* and *G*) could only be fitted by double exponential terms, which reflect a two-step binding process. The k_{app} values of the fast step increased linearly with mant-GTP, whereas k_{app} of the slow step was independent of the concentration. For eRF3 alone, the association rate constant for the first step was $k_{+1} = 3.1\ \mu M^{-1}\ s^{-1}$, the rate constant of the following rearrangement $k_{+2} = 3.8\ s^{-1}$, and the dissociation rate constants k_{-1} and k_{-2} were 27 and 3 s^{-1}, respectively (Table 1 and Fig. 7*B*). The resulting K_d value of 7 μM (Table 1) agreed well with the K_d value obtained by equilibrium titration (Fig. 6*D* and Table 1), and was lower than the respective value measured at 2.5 mM Mg^{2+} (Table 1). The K_d value of 47 μM for the binding of unlabeled GTP to eRF3 in the absence of Mg^{2+} (Table 2), which was determined by titrating the eRF3·mant-GTP complex with unlabeled GTP (Fig. 6*E*), was also somewhat lower than the K_d value for the binding of unlabeled GTP to eRF3 in the presence of Mg^{2+} (Table 2). The absence of Mg^{2+} ions, however, had the opposite effect on binding of mant-GTP to eRF3·eRF1. The association rate constant for the first step was $k_{+1} = 3.5\ \mu M^{-1}\ s^{-1}$, the rate constant of the following rearrangement step $k_{+2} = 2.5\ s^{-1}$, and the dissociation rate constants k_{-1} and k_{-2} were 13 and 1.7 s^{-1}, respectively (Table 1 and Fig. 7*B*). The resulting $K_d = 2.4$ μM (Table 1) agreed well with that obtained by equilibrium titration (Fig. 6*I* and Table 1) and was 5–8-fold higher than the respective value measured at 2.5 mM Mg^{2+} (Table 1). Thus, whereas the absence of Mg^{2+} enhanced binding of mant-GTP/GDP to eRF3 alone and of mant-GDP to eRF3·eRF1, binding of mant-GTP to eRF3·eRF1 was, on the contrary, stimulated by Mg^{2+}. The $K_d = 25$ μM for binding of unlabeled GTP to the eRF3·eRF1 complex (Table 2), which was determined by titrating the eRF3·eRF1·mant-GTP complex with unlabeled GTP (Fig. 6*J*), was also substantially higher than the K_d value for the binding of unlabeled GTP to the eRF3·eRF1 complex in the presence of Mg^{2+} (Table 2).

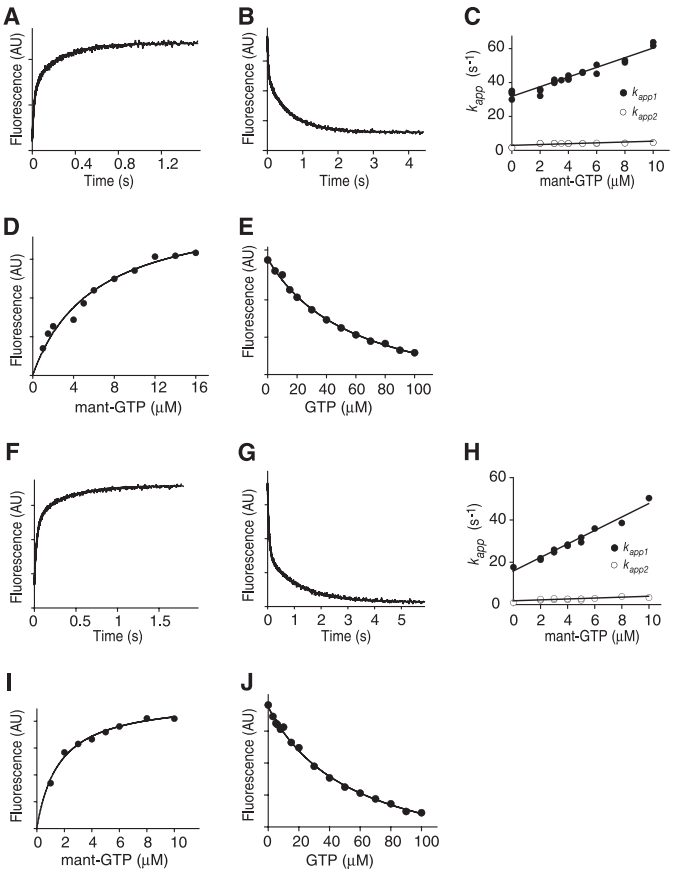

FIGURE 6. **Binding of GTP and mant-GTP to eRF3 alone, and to eRF3 and eRF1 in the absence of Mg^{2+}.** *A*, time course of the association of mant-GTP (4 μM) with eRF3 (0.5 μM). *B*, dissociation of mant-GTP·eRF3 complex (0.5 μM eRF3 and 6 μM mant-GTP) in the presence of GTP (300 μM). The *smooth lines* represent double-exponential fits that yielded the respective rate constants k_{app1} and k_{app2} for the first and second steps, respectively. *C*, concentration dependence of k_{app1} and k_{app2}. *Smooth lines* represent theoretical curves for the first (*filled circles*) and the second (*open circles*) step generated using the values of the elemental rate constants in Table 1. *D*, titration of eRF3 (0.5 μM) with mant-GTP. The *solid line* shows the fit to the data using a one-site binding model. *E*, chase titration of the eRF3·mant-GTP complex (0.8 μM eRF3 and 3 μM mant-GTP) with GTP. *Solid line* represents the result of the fit, as described under "Experimental Procedures." *F*, time course of the association of mant-GTP (5 μM) and 0.5 μM eRF3 in the presence of eRF1 (5 μM). *G*, dissociation of the mant-GTP·eRF3·eRF1 complex (0.5 μM eRF3, 5 μM eRF1, 5 μM mant-GTP) in the presence of GTP (250 μM). The *smooth lines* represent double-exponential fits. *H*, concentration dependence of k_{app1} and k_{app2}. *Smooth lines* represent theoretical curves for the first (*filled circles*) and the second (*open circles*) step generated using the values of the elemental rate constants in Table 1. *I*, titration of the eRF3·eRF1 complex (0.5 μM eRF3, 5 μM eRF1) with mant-GTP. The *solid line* shows the fit to the data using a one-site binding model. *J*, chase titration of the eRF1·eRF3·mant-GTP complex (0.8 μM eRF3, 8 μM eRF1, and 3 μM mant-GTP) with GTP. *Solid line* represents the result of the fit, as described under "Experimental Procedures."

DISCUSSION

In this report we describe a kinetic and thermodynamic analysis of the interaction of eRF3 with guanine nucleotides in the absence and in the presence of eRF1 and 80 S ribosomes. The association and dissociation rate constants of guanine nucleotide binding to eRF3 were measured using the fluorescent guanine nucleotide derivatives mant-GTP/GDP, and the equilibrium dissociation constants were determined both for unlabeled GTP/GDP and for their mant-derivatives. In most cases, very similar K_d values were obtained for mant-labeled and unmodified nucleotides, indicating that the nucleotide binding properties of the factors were not affected by the mant group; in three cases where the affinity was particularly low, it was moderately increased by the presence of the mant group. This suggests that the interactions of the mant group with the protein are too weak to contribute to the affinity of tight complexes, and may become apparent only when the complexes are intrinsically unstable.

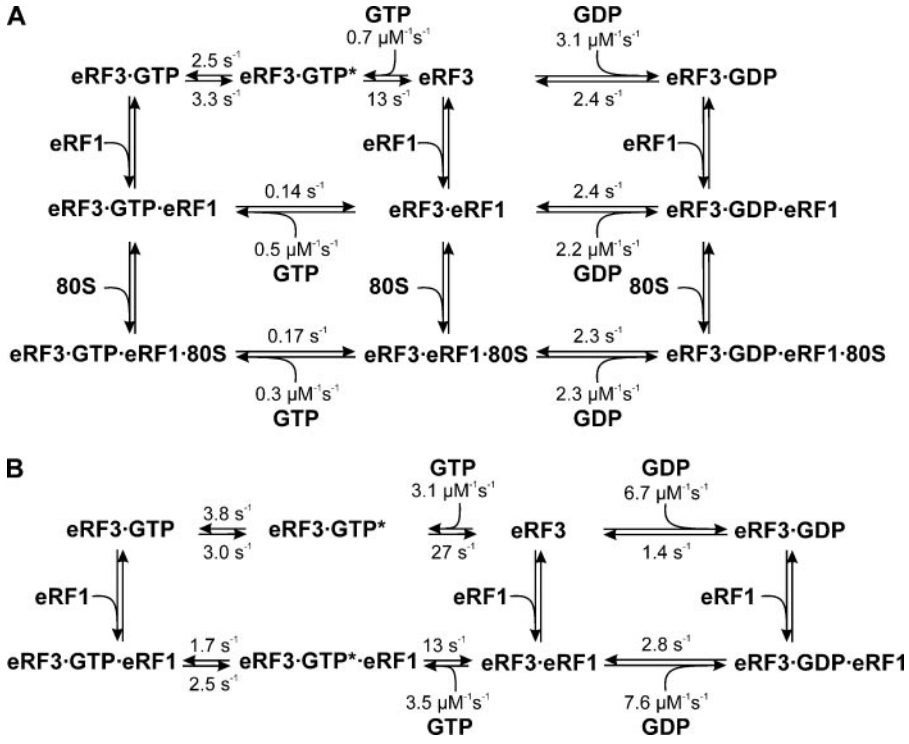

FIGURE 7. **The kinetic scheme of the interaction of eRF3 with guanine nucleotides.** *A*, in the presence of 2.5 mM Mg^{2+}. *B*, in the absence of Mg^{2+}.

We found that at the physiological Mg^{2+} concentration of 2.5 mM, K_d values for binding of GDP and GTP to eRF3 alone were about 1 μM and 70 μM, respectively. Thus, the affinity of eRF3 for GTP is almost two orders of magnitude lower than for GDP. The K_d values obtained in the present study by equilibrium titration and kinetic methods agree well with recently reported values (19), with the exception of the K_d of the eRF3·GTP complex, which was lower than that determined by nitrocellulose filtration (19). Most probably, the main reason for the latter discrepancy is the use of a non-equilibrium detection method (19), which could result in an artificially high dissociation constant for the labile complex. It was shown that filtration, being a nonequilibrium technique, tends to produce artifacts when rapid reactions and/or weak complexes are investigated (32–35). Whereas the kinetics of mant-GDP binding to eRF3 was consistent with a one-step binding mechanism, the interaction of eRF3 with mant-GTP was more complex, and double-exponential time courses were indicative of a two-step binding process in which the initial association of mant-GTP and eRF3 is followed by a conformational change. Because the k_{+1} values in all cases were much lower than the expected diffusion-controlled association rate constants, an additional initial rapid equilibrium binding step cannot be excluded (36). However, if it exists, this step must be readily reversible and does not contribute appreciably to the affinity of the complexes.

Both mant-guanine nucleotides dissociated rapidly from eRF3 with the rates of 2.4 s^{-1} for mant-GDP and 3.3 s^{-1} for the rate-limiting step for mant-GTP dissociation. Consistent with the previously reported data (18), the affinity of GDP to eRF3 alone was higher in the absence of Mg^{2+} ($K_d = 0.13$ μM). However, in contrast to the same report (18) but consistent with recent data (19), the affinity of eRF3 to GDP was high ($K_d \sim 1.3$ μM) also in the presence of 2.5 mM Mg^{2+}, and the absence of Mg^{2+} did not appreciably affect the affinity of eRF3 to GTP ($K_d \sim 45$ μM in the absence, compared with ~70 μM in the presence of Mg^{2+}).

eRF1 and eRF3 form a tight complex, both in the presence and in the absence of guanine nucleotides. Whereas eRF1 did not influence binding of eRF3 to GDP (either in the presence or in the absence of 2.5 mM Mg^{2+}), association of eRF3 with eRF1 at 2.5 mM Mg^{2+} resulted in formation of the eRF1·eRF3 complex, which had a high affinity to GTP ($K_d \sim 0.7$ μM). The increase in affinity for GTP in the ternary eRF1·eRF3·GTP complex indicates that the interaction affinity between eRF1 and eRF3 also increased by the same degree, *i.e.* a factor of 100. At high concentrations of proteins, both the binary eRF1·eRF3 and ternary eRF1·eRF3·GTP complexes are stable and can be isolated by gel filtration; however, the difference in affinities may become apparent at low factor concentrations. This would explain the apparent requirement for GTP of eRF1/eRF3 association reported when studied by immunoprecipitation (37), which is a non-equilibrium method with a strong bias toward isolating high affinity complexes.

In kinetic experiments, association of eRF3 with eRF1 in the presence of 2.5 mM Mg^{2+} lowered the dissociation rate constant for mant-GTP ~24-fold. The stimulatory effect of eRF1 on binding of eRF3 to GTP strongly depended on the presence of Mg^{2+}. Thus, in the absence of Mg^{2+}, association of eRF3 with eRF1 resulted in only a 2-fold increase of the affinity of eRF3 to GTP ($K_d \sim 25$ μM). 80 S ribosomes did not appreciably influence either binding of guanine nucleotides to the eRF1·eRF3 complex or GDP/GTP exchange on it, in notable contrast to bacterial ribosomes, which were reported to accelerate GDP exchange on RF3 (15).

Taken together, our data therefore indicate that the mechanism of guanine nucleotide exchange on eRF3 differs fundamentally from that on prokaryotic RF3 and that in addition to inducing peptide release and GTP hydrolysis (17), the mutual interdependence of eRF1 and eRF3 in termination also involves guanine nucleotide binding to eRF3. Taking into consideration that GTP is present in a ~10-fold molar excess over GDP in the cytosol (38), but that eRF3 has a ~100-fold higher affinity to GDP than to GTP, we suggest that in the cytoplasm, any eRF3 that is not associated with eRF1 will exist in a GDP-bound form. However, at physiological Mg^{2+} concentrations, the affinity of the eRF1·eRF3 complex to GTP is even slightly higher than to GDP, and the dissociation of GTP from the complex is much slower than of GDP, so that eRF3 will predominantly be bound

to GTP in a relatively long-lived eRF1·eRF3·GTP ternary complex. The important implication of this finding is that eRF1 and eRF3 most likely bind to the ribosomal A site of pretermination complexes as a ternary complex with GTP, in analogy to the eEF1A·GTP·aminoacyl-tRNA complex, as first suggested by Nakamura *et al.* (39). This proposal is consistent with the structural similarity between eRF3 and eEF1α (9, 18, 40) and the similar shapes of tRNA and eRF1 (41). According to a recent model for translation termination in eukaryotes (17), hydrolysis of GTP by eRF3 is required for, and therefore is likely to precede, the hydrolysis of peptidyl-tRNA. It is not known whether eRF3-GDP dissociates from the ribosome after GTP hydrolysis or whether it remains associated with the complex until peptidyl-tRNA is hydrolyzed and then dissociates from the post-termination complex as a complex with eRF1. However, even if eRF3-GDP dissociates from the post-termination ribosome alone, GDP/GTP exchange on eRF3 would occur readily as soon as eRF3 binds again to eRF1.

The mechanism of nucleotide binding/exchange on eRF3 and the role of eRF1 are very distinct among GTP-binding proteins. In most GTPases, such as small Ras-like GTPases, heterotrimeric G proteins, and EF-Tu, GTP/GDP binding is stabilized by a Mg^{2+} ion that is coordinated by elements of switch I and switch II regions (31). The intrinsic GDP dissociation from these proteins is very slow, limiting GTP binding, and specific GEFs are therefore required to accelerate nucleotide exchange to physiologically relevant rates. The structures of GEFs are diverse, but they all involve disruption of the nucleotide binding site by disturbing structural elements that interact with the guanine base and the β-phosphate and by opening the switch I and switch II regions; this results in the destabilization of Mg^{2+} binding, which in turn promotes GDP dissociation (42). However, for a few proteins, such as the Ffh component of the bacterial signal recognition particle (SRP), Mg^{2+} does not contribute significantly to the affinity of GTP/GDP binding, and exchange of nucleotides is rapid and spontaneous (43). Similar considerations may apply to translation factors such as IF2 and EF-G for which no GEFs have been identified. Similarly, Mg^{2+} does not stabilize GDP binding to eRF3 alone or to its complex with eRF1, and a GEF is not required for rapid GDP dissociation from any form of the factor. eRF1 clearly does not act like a classical GEF, which increases the dissociation of GDP from a GTPase, but rather shows characteristics reminiscent of another group of GTPase regulatory proteins, GDP-dissociation inhibitors (GDIs), which stabilize the binding of GDP to the Rho and Rab GTPase subfamilies (44). Crystallographic analysis of Rac2-LyGDI and Cdc42-RhoGDI complexes (45, 46) indicates that the regulatory domain of the GDI binds to the switch I and switch II regions of the GTPase, competing with GEF proteins but importantly also stabilizing precisely those elements of the Mg^{2+} ion coordination network that are disrupted by GEFs (47, 48). Consequently, RhoGDI likely inhibits GDP dissociation from Rac2 and Cdc42 by stabilizing the switch I-mediated binding of the Mg^{2+} ion in the GDP conformation of the proteins and possibly also by preventing conformational changes in switch II that would disrupt the coordination of the Mg^{2+} ion. Another example for guanine nucleotide stabilization was found in the SRP-related GTPases, Ffh and FtsY, which interact via their GTP binding domains and reciprocally stimulate the GTPase activities of one another (49). In analogy to what we have observed for the eRF3-eRF1 complex, only the affinity for GTP was increased in the complex, whereas the affinity for GDP remained unchanged (50). However, the important difference between the Rho-RhoGDI and Ffh-FtsY complexes compared with eRF3-eRF1 is that in the former cases the contacts and consequently the effects on nucleotide binding are mediated by the G domains of these GTPases and involve their respective nucleotide binding pockets (51–53). In contrast, modulation by the eRF1 of eRF3 affinity for GTP is indirect and is mediated through their respective interacting C-terminal domains. However, direct contact of the G domain of eRF3 with some other regions of eRF1 cannot be excluded at present.

The crystal structure of yeast eRF3 (18) offers an attractive hypothesis for the mechanism, by which eRF1 might stabilize the binding of GTP to eRF3. The structures of the GTP binding domain 1 and the β-barrel domains 2 and 3 of eRF3 are similar to the respective domains of EF-Tu and eEF1α, but the orientation of domain 1 relative to domains 2 and 3 in eRF3 and in eEF1α/EF-Tu·GDP differ by 144° (40, 54). In contrast to EF-Tu, Mg^{2+} is not apparent in the eRF3 crystal structure and the switch I and switch II elements that usually coordinate Mg^{2+} binding in G domains are either disordered (switch I) or, over limited regions, oriented differently compared with equivalent residues in EF-Tu, and are too far from the Mg^{2+} binding site to coordinate the ion (switch II). Sequence conservation and mutational analyses suggest that eRF1 binds to eRF3 near the domain 2/domain 3 interface, adjacent to domain 1 (18). We suggest that the binding of eRF1 to eRF3 may influence the position of domain 1 relative to domains 2/3 and induce a rearrangement of domain 1 that stabilizes the ordered conformation of the switch I and switch II elements such that they better coordinate the Mg^{2+} ion. Our observation that the stimulatory effect of eRF1 on binding of eRF3 to GTP depends on the presence of Mg^{2+} is consistent with this suggestion. If eRF1 indeed stabilizes binding of Mg^{2+} to eRF3, then such stabilization could also be responsible for eRF1 activity in stimulating GTP hydrolysis by eRF3 on the ribosome (10, 11), because Mg^{2+} is essential for this process for many GTPases (31, 42). Atomic structures of eRF1·eRF3 complexes with different guanine nucleotides are required to identify structural changes in the switch I and switch II regions of eRF3 caused by eRF1 that are responsible for eRF1 stimulation of GTP binding to eRF3.

Acknowledgments—We thank Natasha Wallace for expert technical assistance, and L. L. Kisselev and L. Yu. Frolova for the generous gift of eRF1 and eRF3 expression vectors.

REFERENCES

1. Kisselev, L., Ehrenberg, M., and Frolova, L. (2003) *EMBO J.* **22,** 175–182
2. Klaholz, B. P., Pape, T., Zavialov, A. V., Myasnikov, A. G., Orlova, E. V., Vestergaard, B., Ehrenberg, M., and van Heel, M. (2003) *Nature* **421,** 90–94
3. Rawat, U. B., Zavialov, A. V., Sengupta, J., Valle, M., Grassucci, R. A., Linde, J., Vestergaard, B., Ehrenberg, M., and Frank, J. (2003) *Nature* **421,** 87–90

4. Petry, S., Brodersen, D. E., Murphy, F. V. 4th, Dunham, C. M., Selmer, M., Tarry, M. J., Kelley, A. C., and Ramakrishnan, V. (2005) *Cell* **123,** 1255–1266
5. Frolova, L. Y., Tsivkovskii, R. Y., Sivolobova, G. F., Oparina, N. Y., Serpinsky, O. I., Blinov, V. M., Tatkov, S. I., and Kisselev, L. L. (1999) *RNA* **5,** 1014–1020
6. Zavialov, A. V., Mora, L., Buckingham, R. H., and Ehrenberg, M. (2002) *Mol. Cell* **10,** 789–798
7. Milman, G., Goldstein, J., Scolnick, E., and Caskey, T. (1969) *Proc. Natl. Acad. Sci. U. S. A.* **63,** 183–190
8. Zhouravleva, G., Frolova, L., Le Goff, X., Le Guellec, R., Inge-Vechtomov, S., Kisselev, L., and Philippe, M. (1995) *EMBO J.* **14,** 4065–4072
9. Inagaki, Y., and Doolittle, W. F. (2000) *Mol. Biol. Evol.* **17,** 882–889
10. Frolova, L. Y., Merkulova, T. I., and Kisselev, L. L. (2000) *RNA* **6,** 381–390
11. Frolova, L., Le Goff, X., Zhouravleva, G., Davydova, E., Philippe, M., and Kisselev, L. (1996) *RNA* **2,** 334–341
12. Frolova, L. Y., Simonsen, J. L., Merkulova, T. I., Litvinov, D. Y., Martensen, P. M., Rechinsky, V. O., Camonis, J. H., Kisselev, L. L., and Justesen, J. (1998) *Eur. J. Biochem.* **256,** 36–44
13. Ito, K., Ebihara, K., and Nakamura, Y. (1998) *RNA* **4,** 958–972
14. Freistroffer, D. V., Pavlov, M. Y., MacDougall, J., Buckingham, R. H., and Ehrenberg, M. (1997) *EMBO J.* **16,** 4126–4133
15. Zavialov, A. V., Buckingham, R. H., and Ehrenberg, M. (2001) *Cell* **107,** 115–124
16. Salas-Marco, J., and Bedwell, D. M. (2004) *Mol. Cell Biol.* **24,** 7769–7778
17. Alkalaeva, E. Z., Pisarev, A. V., Frolova, L. Y., Kisselev, L. L., and Pestova, T. V. (2006) *Cell* **125,** 1125–1136
18. Kong, C., Ito, K., Walsh, M. A., Wada, M., Liu, Y., Kumar, S., Barford, D., Nakamura, Y., and Song, H. (2004) *Mol. Cell* **14,** 233–245
19. Hauryliuk, V., Zavialov, A., Kisselev, L., and Ehrenberg, M. (2006) *Biochimie* (*Paris*) **88,** 747–757
20. Pestova, T. V., Hellen, C. U. T., and Shatsky, I. N. (1996) *Mol. Cell Biol.* **16,** 6859–6869
21. Pestova, T. V., Shatsky, I. N., Fletcher, S. P., Jackson, R. J., and Hellen, C. U. T. (1998) *Genes Dev.* **12,** 67–83
22. Pestova, T. V., Lomakin, I. B., Lee, J. H., Choi, S. K., Dever, T. E., and Hellen, C. U. T. (2000) *Nature* **403,** 332–335
23. Frolova, L., Seit-Nebi, A., and Kisselev, L. (2002) *RNA* **8,** 129–136
24. Pestova, T. V., and Hellen, C. U. T. (2003) *Genes Dev.* **17,** 181–186
25. Gill, S. C., and von Hippel, P. H. (1989) *Anal. Biochem.* **182,** 319–326
26. Hemsath, L., and Ahmadian, M. R. (2005) *Methods* **37,** 173–182
27. Fersht, A. (1999) *Structure and Mechanism in Protein Science: A Guide to Enzyme Catalysis and Protein Folding*, p. 151, W. H. Freeman and Company, New York
28. John, J., Sohmen, R., Feuerstein, J., Linke, R., Wittinghofer, A., and Goody, R. S. (1990) *Biochemistry* **29,** 6058–6065
29. Rodnina, M. V., Fricke, R., Kuhn, L., and Wintermeyer, W. (1995) *EMBO J.* **14,** 2613–2619
30. Hiratsuka, T. (1983) *Biochim. Biophys. Acta* **742,** 496–508
31. Sprang, S. R. (1997) *Annu. Rev. Biochem.* **66,** 639–678
32. Berger, B., Prinz, H., Striessnig, J., Kang, H. C., Haugland, R., and Glossmann, H. (1994) *Biochemistry* **33,** 11875–11883
33. Lenzen, C., Cool, R. H., Prinz, H., Kuhlmann, J., and Wittenghofer, A. (1998) *Biochemistry* **37,** 7420–7430
34. Gromadski, K. B., Wieden, H.-J., and Rodnina, M. V. (2002) *Biochemistry* **41,** 162–169
35. Wilden, B., Savelsbergh, A., Rodnina, M. V., and Wintermeyer, W. (2006) *Proc. Natl. Acad. Sci. U. S. A.* **103,** 13670–13675
36. Moser, C., Mol, O., Goody, R. S., and Sinning, I. (1997) *Proc. Natl. Acad. Sci. U. S. A.* **14,** 11339–11344
37. Kobayashi, T., Funakoshi, Y., Hoshino, S., and Katada, T. (2004) *J. Biol. Chem.* **279,** 45693–45700
38. Traut, T. W. (1994) *Mol. Cell Biochem.* **140,** 1–22
39. Nakamura, Y., Ito, K., and Isaksson, L. A. (1996) *Cell* **87,** 147–150
40. Andersen, G. R., Pedersen, L., Valente, L., Chatterjee, I., Kinzy, T. G., Kjeldgaard, M., and Nyborg, J. (2000) *Mol. Cell* **6,** 1261–1266
41. Nakamura, Y., and Ito, K. (2003) *Trends Biochem. Sci.* **28,** 99–105
42. Vetter, I. R., and Wittinghofer, A. (2001) *Science* **294,** 1299–1304
43. Jagath, J. R., Rodnina, M. V., Lentzen, G., and Wintermeyer, W. (1998) *Biochemistry* **37,** 15408–15413
44. DerMardirossian, C., and Bokoch, G. M. (2005) *Trends Cell Biol.* **15,** 356–363
45. Hoffman, G. R., Nassar, N., and Cerione, R. A. (2000) *Cell* **100,** 345–356
46. Scheffzek, K., Stephan, I., Jensen, O. N., Illenberger, D., and Gierschik, P. (2000) *Nat. Struct. Biol.* **7,** 122–126
47. Li, R., and Zheng, Y. (1997) *J. Biol. Chem.* **272,** 4671–4679
48. Wei, Y., Zhang, Y., Derewenda, U., Liu, X., Minor, W., Nakamoto, R. K., Somlyo, A. V., Somlyo, A. P., and Derewenda, Z. S. (1997) *Nat. Struct. Biol.* **4,** 699–703
49. Powers, T., and Walters, P. (1995) *Science* **269,** 1422–1424
50. Peluso, P., Shan, S.-U., Nock, S., Herschlag, D., and Walter, P. (2001) *Biochemistry* **40,** 15224–15233
51. Egea, P. F., Shan, S. O., Napetschnig, J., Savage, D. F., Walter, P., and Stroud, R. M. (2004) *Nature* **427,** 215–221
52. Focia, P. J., Shepotinovskaya, I. V., Seidler, J. A., and Freymann, D. M. (2004) *Science* **303,** 373–377
53. Shan, S. O., Stroud, R. M., and Walter, P. (2004) *PLoS Biology* **2,** 1572–1581
54. Song, H., Parsons, M. R., Rowsell, S., Leonard, G., and Phillips, S. E. (1999) *J. Mol. Biol.* **285,** 1245–1256